https://doi.org/10.1007/s41230-025-4083-4

Effect of cooling rate on solidification behavior and micro-segregation of high-alloyed wrought superalloy GH4975

**Guang-di Zhao[1], *Xi-min Zang[2], Yi-xuan Sun[1], and Xiao-yu Yao[3]

1. School of Materials and Metallurgy, University of Science and Technology Liaoning, Anshan 114051, Liaoning, China

2. School of Materials Science and Engineering, Shenyang University of Technology, Shenyang 110870, China

3. Institute of Metal Research, Chinese Academy of Sciences, Shenyang 110016, China

Copyright © 2025 Foundry Journal Agency

Abstract: The high-alloyed wrought superalloy GH4975 tends to form coarse MC carbides and eutectic (γ+γ′) phases, which adversely affect the cogging and homogenization process. To provide theoretical guidance for control of MC carbides and eutectic (γ+γ′) formation, differential thermal analysis (DTA) was utilized to investigate the effect of cooing rate (10–90 °C·min^{-1}) on solidification behavior and micro-segregation of GH4975 alloy. According to the thermodynamic calculation and distribution characteristics of precipitates, the MC carbides can act as nucleation sites for γ dendrites, but the nucleation of γ dendrites becomes less dependent on the MC carbide primers at higher cooling rates. As the γ dendrites grow, the elements including Ti and Nb gradually accumulate in the residual liquid and leads to the formation of more MC carbides near the interdendritic region. Finally, the solidification is terminated with the formation of eutectic (γ+γ′). With an increase in cooling rate, the liquidus temperature rises, but the solidus temperature decreases, and thus the solidification range is obviously enlarged. The dendritic structure is significantly refined by the increase of cooling rate. The secondary dendrite arm spacing, λ_2, as a function of cooling rate, $\dot{T}$, can be expressed as $\lambda_2=216.78\dot{T}^{-0.42}$. Moreover, the increasing cooling rate weakens the back diffusion of Al, Ti, and Nb, increases the undercooling, and limits the growth of precipitates. Consequently, the sizes of MC carbides, eutectic (γ+γ′), and primary γ′ significantly decrease, but the area fraction of eutectic (γ+γ′) linerly increases as the cooling rate rises. Thus moderate cooling rate (such as 30 °C·min^{-1}) should be selected during the solidification process of GH4975 alloy.

Keywords: Ni-based superalloy; cooling rate; solidification segregation; MC carbides; eutectic (γ+γ′)

CLC numbers: TG146.1+5 **Document code:** A **Article ID:** 1672-6421(2026)01-083-11

1 Introduction

Ni-based GH4975 (Russian ЭП975) represents a new γ′ precipitation-hardened wrought superalloy with superior high-temperature strength and creep resistance. Predominantly, it is utilized in the fabrication of high-performance aeroengine turbine discs[1]. The alloying degree of GH4975 alloy is extremely high, and the total content of (Al+Ti+Nb) is approximately 9.2wt.%. Therefore, the mass fraction of γ′ in the aging state can reach up to 64%, and the long-term service temperature of this alloy is as high as 850–950 °C[2]. However, the high alloying degree significantly increases the deformation resistance and worsens the hot ductility. It is currently recognized as the highest alloyed disk alloy that can be processed using the cast and wrought route[3].

It has been reported that the Nb, Ti, Al, and W exhibit severe segregation during solidification of GH4975 alloy. The Nb, Ti, and Al are segregated in interdendritic regions (positive segregation), while W is segregated in dendrite arms (negative segregation). The MC carbides, eutectic (γ+γ′), and γ′ are the main precipitates in as-cast GH4975 alloy[4, 5]. During the hot deformation of as-cast GH4975 alloy, MC carbides are prone to become the crack initiation source due to their cracking. Furthermore, the stress concentration

*Xi-min Zang

Male, boron in 1978, Professor. His research interests mainly focus on preparation and characterization of special steel, theory and process of electroslag remelting, and intelligent manufacturing of metallurgical processes. E-mail: zangxm@sut.edu.cn

**Guang-di Zhao

E-mail: gdzhao12s@alum.imr.ac.cn

Received: 2024-04-20; Revised: 2024-05-27; Accepted: 2024-09-09

around MC carbides can lead to cracking of γ matrix[5]. Our previous study has found that the coarse eutectic (γ+γ′) is the most effective crack initiation site in the similar high-alloyed superalloy U720Li, and high temperature homogenization treatment is essential to dissolve the eutectic (γ+γ′)[6]. However, coarse eutectic (γ+γ′) is very difficult to dissolve[7, 8], and MC carbides usually remain stable during the homogenization process[9-11]. Therefore, it is necessary to understand how to control the formation of eutectic (γ+γ′) and MC carbides during solidification of GH4975 alloy.

The nucleation and growth of non-equilibrium phases can be modified by adjusting the solidification cooling rate, and numerous studies have been conducted on how the cooling rate influences microstructures and properties of Ni-based superalloys. Gong et al.[12] found that the secondary dendrite arm spacing (SDAS), segregation degree, size and volume fraction of γ′, and the size of eutectic (γ+γ′) in K417G alloy increased with decreasing the cooling rate from 85.2 °C·min^{-1} to 50.4 °C·min^{-1}, but the eutectic (γ+γ′) volume fraction showed a decreasing trend. The specimen with the lowest cooling rate possessed the best mechanical properties. El-Bagoury et al.[13] studied the influence of cooling rates (1 °C·min^{-1}, 10 °C·min^{-1}, and 100 °C·min^{-1}) on the solidification process of Inconel718 alloy. They found that the onset temperature of eutectic phase precipitation decreased, and the NbC volume fraction increased with increasing cooling rate. Milenkovic et al.[14] found that the MAR-IVI247 alloy showed cellular structure at the cooling rate of 15 °C·min^{-1} and dendritic structure at 60 °C·min^{-1} , 300 °C·min^{-1}, and 600 °C·min^{-1}. The microstructure also changed with cooling rates: At a cooling rate of 15 °C·min^{-1}, the microstructure consisted of a γ/γ′ matrix with carbides and eutectic (γ+γ′). When cooled at a rate of 60 °C·min^{-1}, the microstructure was composed of a γ/γ′ matrix with carbides. At higher cooling rates of 300 °C·min^{-1}, and 600 °C·min^{-1}, the microstructure included a γ/γ′ matrix with MC carbides and eutectic (γ+MC). Moreover, as the cooling rates increased, the SDAS decreased, while the hardness of the alloy increased. Ling et al.[15] studied the transformation rate of solid phase in Inconel718 alloy at the cooling rates of 6 °C·min^{-1} to 840 °C·min^{-1}, and found that when the cooling rate was 180 °C·min^{-1}, the amount of Laves phase reached the maximum value, because the cooling rate has opposite effect on the SDAS and solidification time. Shi et al.[16] found that as the cooling rate decreased from 20 °C·min^{-1} to 5 °C·min^{-1}, the constitutional supercooling at solidification front had more significant influence on the solid-liquid interface, and the amount and size of Laves phase increased. As the cooling rates intensified, the concentrations of Ni, Cr, Fe, and Al within the dendrite core underwent a slight decline, whereas the concentrations of Nb, Mo, and Ti experienced a notable increase. Above all, the solidification cooling rate definitely has a significant influence on the homogenization process and thermal plasticity of Ni-based superalloys.

The GH4975 alloy ingot is usually prepared by vacuum induction melting (VIM) plus vacuum arc remelting (VAR) processes[4, 5]. The development of aeroengine turbine disc industry has the demand for larger-sized GH4975 ingots. During the solidification, variations in the melting process and the distance from mold wall can inevitably lead to different cooling rates. The larger ingot diameter can cause a much slower cooling rate in the inner section of the ingot, which will dramatically expand the cooling rate difference between the inner section and surface[17]. Therefore, the differential thermal analysis was utilized in this study to investigate how the cooling rate affects the solidification behavior and microstructure of GH4975 alloy. The results are helpful for revealing the solidification segregation and microstructural evolution in large GH4975 ingots. Furthermore, it can provide theoretical guidance for controlling the cooling conditions during production of large-scale, high-alloyed wrought superalloy ingots.

2 Experimental procedure

The GH4975 melt was prepared in a 25 kg vacuum induction melting (VIM) furnace from pure Ni (99.98% purity), Al (99.99% purity), Ti (99.84% purity), Cr (99.24% purity), Co (99.95% purity), W (99.95% purity), Mo (99.99% purity), Nb (99.99% purity), and graphite sheets, and was poured at about 1,430 °C into a cast iron mold to produce an ingot weighing 6.5 kg. The chemical composition of the ingot was determined by iCAP 6300 inductively coupled plasma-atomic emission spectrometry (ICP-AES), and the result is shown in Table 1.

Table 1: Chemical compositions of experimental alloy (wt.%)

C	Al	Ti	Cr	Co	Nb	Mo	W	Ni
0.12	4.99	2.59	7.98	15.7	1.57	1.19	10.01	Bal.

The JMatPro software based on thermodynamic calculations was applied to predict the equilibrium phases precipitation behavior, including possible types of precipitates, precipitation temperature, and solidification temperature ranges.

A cubic sample with dimensions of 10 mm×10 mm×10 mm was cut from half radius of the ingot (Sample A in Fig. 1). The sample was polished mechanically after grinding, and then etched electrolytically in a solution of 13 mL H_3PO_4 + 42 mL HNO_3+43 mL H_2SO_4 under DC 2V for 3–4 s. This electrolyte is mainly used for corrosion of γ matrix, which can highlight the precipitates such as γ′ and MC carbides. It has been used in the studies for microstructural observation of the similar γ′ precipitation-hardened wrought superalloy U720Li[6, 8]. The microstructure was observed under the optical microscopy (OM) and Zeiss-IGMA HD field emission scanning electron microscopy (FESEM). Chemical compositions of the

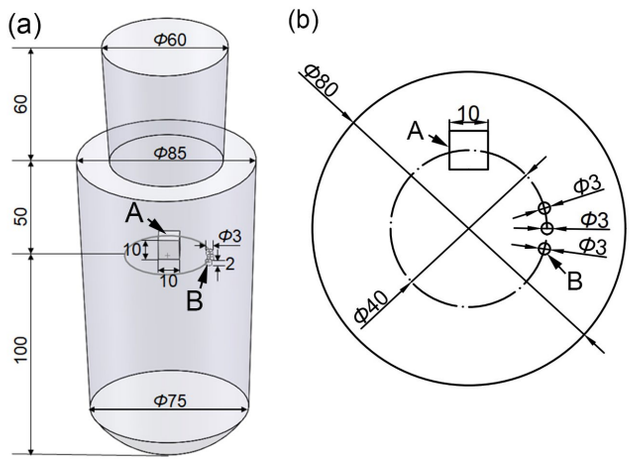

Fig. 1: Schematics of sampling positions and sizes in the ingot (unit: mm): (a) stereoscopic view; (b) cross section view

nonequilibrium phases, i.e., eutectic (γ+γ′) and MC carbides, and element distributions in the interdendritic region were examined by the energy dispersive spectrometry (EDS) attached to the FESEM.

The influence of cooling rate on solidification behavior of GH4975 alloy was investigated by means of differential thermal analysis (DTA). Cylindrical samples of *Φ*3 mm×2 mm were also cut from the half radius of the ingot (Sample B in Fig. 1). All surfaces of these samples were ground down to 400-grit SiC paper and cleaned ultrasonically. Then, these samples were placed in a high-purity alumina crucible and tested in an argon atmosphere from 900 to 1,400 °C after drying. The cooling rates were set to 10 °C·min^{-1}, 30 °C·min^{-1}, and 90 °C·min^{-1}, and the heating rates of all conditions were set to 10 °C·min^{-1}.

Subsequently, the solidified DTA samples were polished and etched using the same method as the as-cast sample above. The microstructures were observed under the OM and SEM. Area fractions of the eutectic (γ+γ′) and MC carbides were determined quantitatively using Image-Pro Plus 6.0 software, the SDAS, and sizes of eutectic (γ+γ′), MC carbides, and γ′ were measured using the Nano Measurer 1.2 software. At least five optical micrographs (×200) were taken from each sample to obtain the average values to guarantee the accuracy of measured results. Note that the area fractions of precipitates in superalloys are usually used to represent their volume fractions[18, 19].

Chemical compositions of the dendrite core, interdendritic region, eutectic (γ+γ′), and MC carbides in the solidified DTA samples were examined by the EDS (rectangular region X-ray acquisition) to clarify how the cooling rate influences the micro-segregation. More than five measurements were used to calculate the average values. In addition, the segregation ratio (SR) defined as the ratio of interdendritic region to dendrite core compositions was introduced to describe the degree of micro-segregation. If the SR of an alloying element is greater than 1, it means that this element exhibits positive segregation, otherwise it means negative segregation.

3 Results

3.1 Thermodynamic calculations and as-cast microstructure

Figure 2 shows the relationship between temperature and mass fractions of the main equilibrium precipitates in GH4975 alloy calculated using JMatPro software. It can be seen that the onset temperature of MC carbides precipitation is about 1,380 °C and that of γ matrix formation is about 1,362 °C, indicating that the MC carbides should precipitate earlier than the γ matrix during solidification. When the temperature decreases to about 1,230 °C, the γ′ phase starts to precipitate, indicating that the precipitation temperature of γ′ in GH4975 alloy is much higher than that of the similar alloy U720Li, which is 1,153 °C[20]. In addition, as the temperature is further decreased to about 1,027 °C, the M_6C carbide can be precipitated.

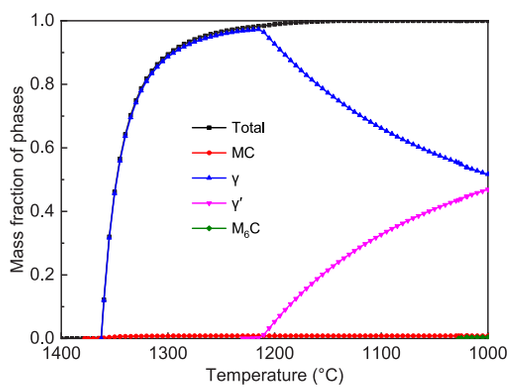

Fig. 2: Relationship between temperature and mass fractions of the main equilibrium precipitates in GH4975 alloy calculated by JMatPro

Figure 3 shows the as-cast microstructure of GH4975 alloy under OM and SEM-BSE (back scattered electron image). It can be seen that the dendritic structure is well developed, as shown in Fig. 3(a). Many coarse elliptical eutectic (γ+γ′) particles are formed in the interdendritic region, as shown in Figs. 3(b) and (c), which indicates that the solidification is terminated with the eutectic (γ+γ′) precipitation. Lots of blocky and elongated MC carbides are precipitated in as-cast GH4975 alloy. Most of the MC carbides are formed near the interdendritic region surrounding the eutectic (γ+γ′) [Fig. 3(a)], and some carbide particles are formed in the dendrite arm and dendrite core, as indicated in Fig. 3(b). This suggests that some MC carbide particles precipitate earlier (consistent with the JMatPro calculation) and can act as nucleation sites for γ dendrites, while the others precipitate later than the γ dendrite but earlier than the eutectic (γ+γ′). Higher magnification observations indicate that lots of fine cubic primary γ′ particles are precipitated in the dendrite core, as shown in Fig. 3(d), and many coarser dendritic primary γ′ are precipitated in the interdendritic region around eutectic (γ+γ′), as seen in Fig. 3(e). Moreover, some extremely fine spherical secondary γ′ are precipitated in the γ matrix between coarse primary γ′ particles in the interdendritic region [Fig. 3(f)], which is in agreement with Ref. [5].

Quantitative and statistical analysis indicate that the average area fraction and diameter of eutectic (γ+γ′) are (0.77±0.09)% and (12.94±6.44) μm, respectively; the average area fraction, length, width, and aspect ratio (length/width) of MC carbides are (0.94±0.22)%, (9.18±5.68) μm, (3.15±1.88) μm, and 2.91, respectively. Compared to other wrought superalloys, the area fraction of eutectic (γ+γ′) in as-cast GH4975 is notably lower than that in as-cast U720Li alloy, which is 2.12%[8, 21], but that of MC carbides in GH4975 alloy is much greater than that in both U720Li alloy (0.04%) and IN718 alloy (0.50%)[8, 21-23].

Figure 4 presents the EDS spectra of the MC carbides and eutectic (γ+γ′) particles in as-cast GH4975 alloy, and Fig. 5 shows

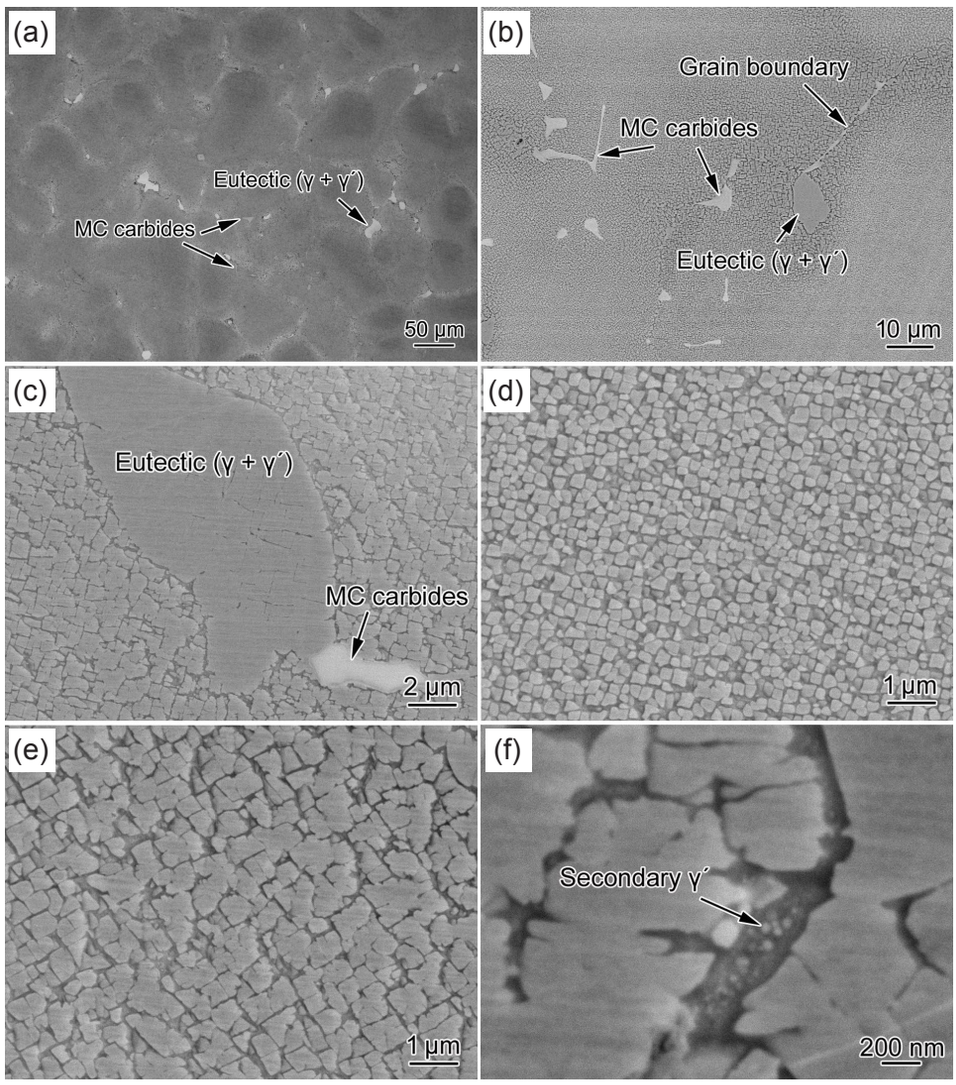

Fig. 3: As-cast microstructure of GH4975 alloy: dendritic structure under OM (a); morphologies of MC carbides (b); and (γ+γ′) eutectics (c) under SEM-BSE; primary γ′ particles precipitated in the dendrite core (d) and interdendritic region (e); and secondary γ′ between coarse primary γ′ in the interdendritic region (f)

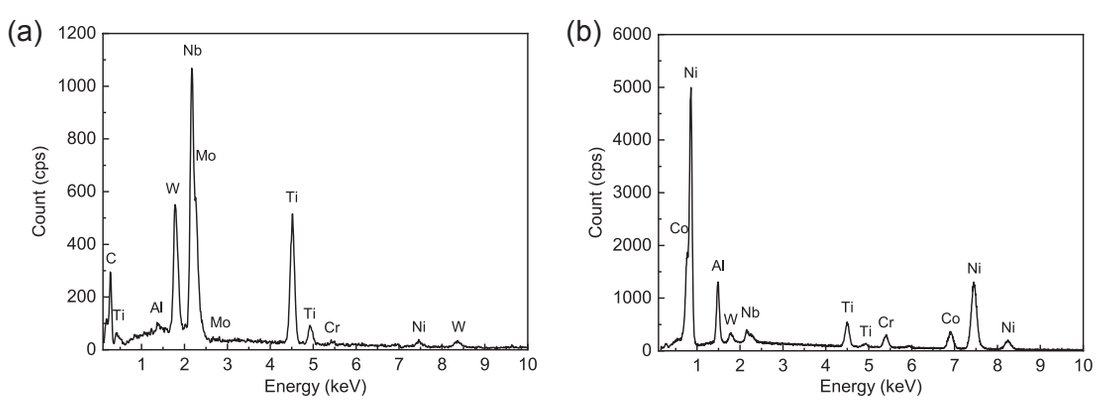

Fig. 4: EDS spectra of the MC carbides (a) and (γ+γ′) eutectics (b) in as-cast GH4975 alloy

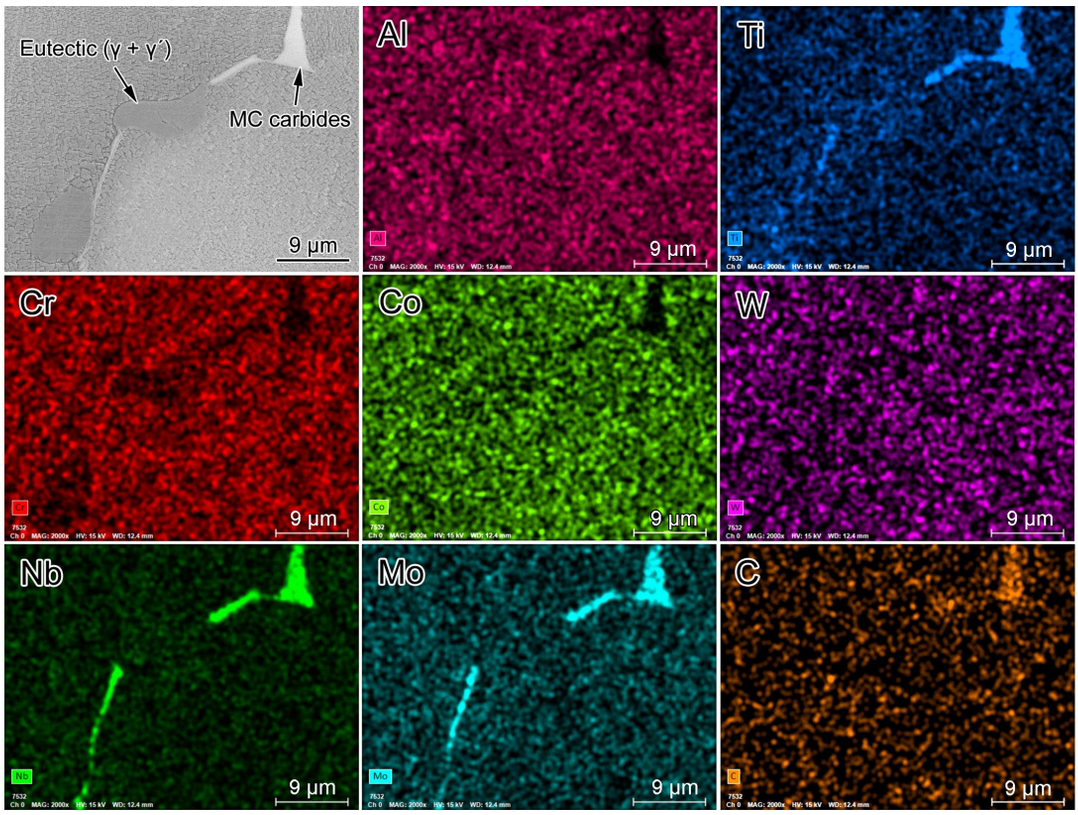

Fig. 5: Element distribution in the interdendritic region of as-cast GH4975 alloy

the elemental distribution maps in the interdendritic region. Obviously, the MC carbides are enriched in C, Nb, Ti, and Mo, but depleted in Al, Cr, and Co. The eutectic (γ+γ′) particles are enriched in Ni, Al, and Ti, but depleted in Cr. This indicates that the primary forming elements for MC carbides are C, Nb, Ti, and Mo, and those for eutectic (γ+γ′) are Ni, Al, and Ti.

3.2 Effect of cooling rate on solidification behavior

Figure 6 shows DTA cooling curves of GH4975 alloy under different solidification cooling rates. At the cooling rates of 10 °C·min^{-1} and 30 °C·min^{-1}, three obvious exothermic peaks (i.e. P-C1, P-C2 and P-C3) are observed in the cooling curves. At the cooling rate of 90 °C·min^{-1}, only two obvious exothermic peaks (i.e. P-C2 and P-C3) exist in the cooling curve. However, a significant slope change appears on the DTA cooling curve with the cooling rate of 90 °C·min^{-1} at about 1,330 °C, which indicates that this should be the peak temperature of P-C1 for this cooling rate. Besides, the height of the exothermic peaks increases significantly with the increase of cooling rate, suggesting that the higher cooling rate leads to a higher phase transformation degree. Through careful comparison, it can be found that at the cooling rate of 10 °C·min^{-1}, the height of P-C2 is lower than that of P-C1, while at the cooling rate of 30 °C·min^{-1}, the height of P-C2 becomes higher than that of P-C1. This suggests that the increase of cooling rate raises the height of P-C2 more significantly. Thus, it can be inferred that as the cooling rate is further increased to 90 °C·min^{-1}, the height of P-C2 will be much higher than that of P-C1 and overlaps the P-C1, causing the fact that the P-C1

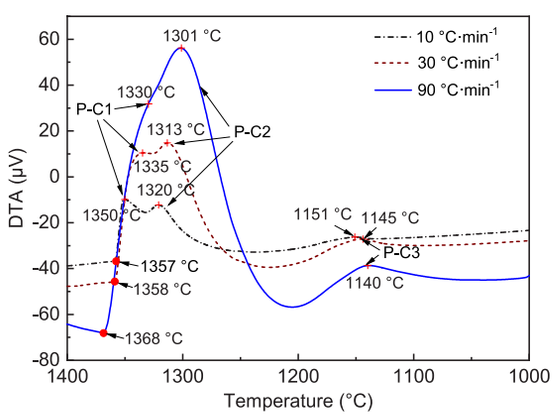

Fig. 6: DTA curves of GH4975 alloy cooled from super-solidus temperature with different cooling rates

could not be clearly observed.

According to the as-cast microstructure observation and the previous studies[4, 5], the third exothermic peak P-C3 associates with the γ′ precipitation. Because some MC carbides precipitate earlier than the γ matrix and become the nucleation sites for the γ dendrites, the first exothermic peak P-C1 should be mainly associated with the growth of γ dendrites nucleated from the MC carbide primers (heterogeneous nucleation) considering that a large amount of heat is released owing to the P-C1. It is not a stretch to infer that the second peak P-C2 nearby the P-C1 should be mainly associated with the formation of the other γ dendrites (homogeneous nucleation). Unfortunately, the exothermic peaks associated with MC carbides and (γ+γ′) eutectics formation are likely to be covered by these two peaks and can not be distinguished.

Table 2 summarizes the initial and peak temperatures of P-C1, the initial, peak, and final temperatures of P-C2, and the peak temperatures of P-C3 on the DTA cooling curves with different cooling rates. It can be seen that the increase of cooling rates markedly raises the initial temperature of P-C1, indicating that the higher cooling rate leads to a higher liquidus temperature. Similar results have been reported in Refs. [24-27]. This is mainly because the increasing cooling rate increases the constitutional supercooling degree in the liquid[27, 28], which promotes the precipitation of γ dendrite nucleation primers MC carbides. Besides, the increasing cooling rate lowers the peak and final temperatures of P-C2 and the peak temperatures of P-C1 and P-C3, suggesting that a higher cooling rate retards the growth of γ dendrites and lowers the precipitation temperature of γ′. The temperature intervals between P-C1 initial temperature and P-C2 final temperature for the cooling rates of 10 °C·min^{-1}, 30 °C·min^{-1}, and 90 °C·min^{-1} are 122 °C, 139 °C, and 164 °C, respectively. This indicates that the solidification range of GH4975 alloy is significantly enlarged by the increasing cooling rate.

Table 2: Summary of solidification reaction temperatures (°C) on DTA curves

Cooling rate	P-C1 initial	P-C1 peak	P-C2 initial	P-C2 peak	P-C2 final	P-C3 peak
10 °C·min^{-1}	1,357	1,350	1,332	1,320	1,235	1,151
30 °C·min^{-1}	1,358	1,335	1,325	1,313	1,219	1,145
90 °C·min^{-1}	1,368	1,330	–	1,301	1,204	1,140

3.3 Effect of cooling rates on microstructure and segregation

Figure 7 shows the dendritic structures of solidified DTA samples with different cooling rates under the OM. It can be seen that the dendritic structure is significantly refined by the increasing cooling rate, which suggests that the nucleation rate of γ dendrite is significantly increased by increasing cooling rates[29]. Hence, the γ dendrite nucleation becomes less dependent on the MC carbide primers at higher cooling rates, and the proportion of homogeneous nucleation increases. Therefore, as the cooling rate increases, the P-C2 on the DTA curves becomes higher and higher than the P-C1, and finally overlaps the P-C1 (Fig. 6). It can also be seen that as the cooling rate increases, the quantities of both MC carbides and (γ+γ′) eutectics increase markedly, and these two phases become finer.

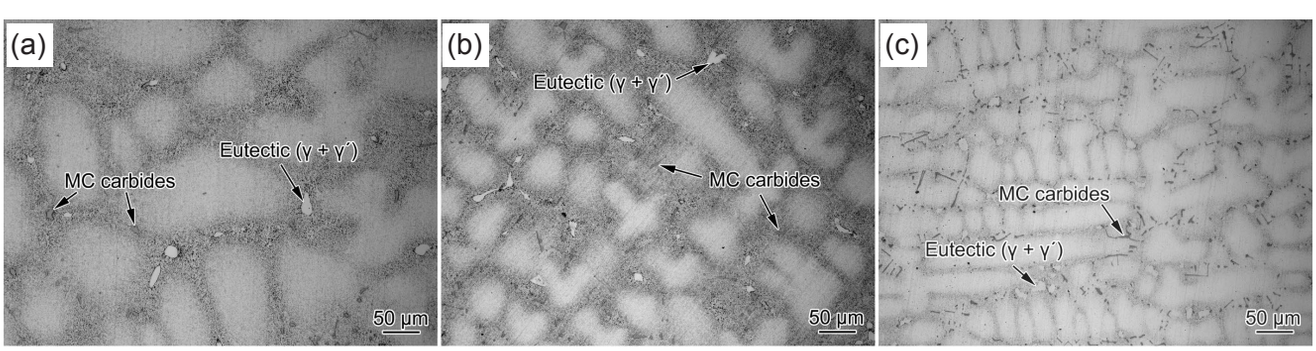

Fig. 7: OM images showing dendritic structures of solidified DTA samples with the cooling rates of 10 °C·min^{-1} (a), 30 °C·min^{-1} (b), and 90 °C·min^{-1} (c)

It is widely known that the SDAS signifies the length of diffusion paths and significantly influences micro-segregation in superalloys[30]. Previous research results have proved that the SDAS (λ_2) can be expressed as a function of cooling rate ($\dot{T}$)[31, 32]:

$$\lambda_2 = \varepsilon \dot{T}^{-n} \quad (1)$$

where ε is a constant and n is the exponent. The ε and n can be modified by the change of cooling rate[33]. The measured SDASs of the solidified DTA samples are shown in Fig. 8, and the fitted curve of SDASs as a function of cooling rate in Eq. (1) can be expressed as:

$$\lambda_2 = 216.78\dot{T}^{-0.42} \quad (2)$$

Apparently, the SDAS decreases gradually with increase of

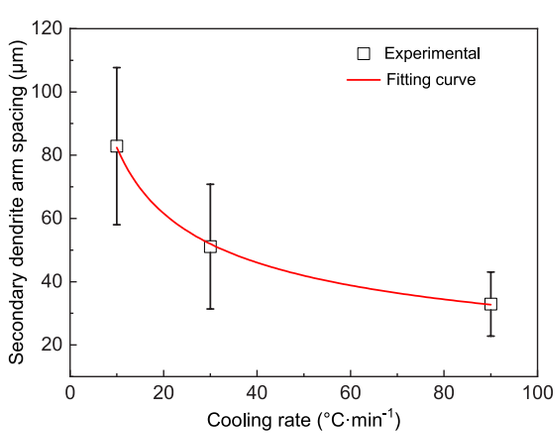

Fig. 8: SDAS of DTA samples as a function of cooling rate

cooling rate. The SDAS of GH4975 alloy ingot was measured to be 59.97±16.13 μm, which is smaller than that at the cooling rate of 10 °C·min^{-1}, but greater than that at the cooling rate of 30 °C·min^{-1}. That is, the solidification cooling rate for the experimental ingot should be located between 10–30 °C·min^{-1}.

Microstructures of the solidified DTA samples were further observed under the SEM-BSE (Fig. 9). The morphologies and distribution characteristics of MC carbides and (γ+γ′) eutectics in the solidified DTA samples are similar to those in the as-cast samples in Figs. 3(b) and (c). The γ′ in interdendritic regions shows interconnected dendritic shape for all the cooling rates, but in the dendrite core, γ′ transforms from irregular shape to cubic shape as the cooling rate increases. Moreover, the γ′ particles in both the interdendritic region and dendrite core are significantly refined with the increase of cooling rate.

The average area fractions and sizes of MC carbides, (γ+γ′) eutectics, and primary γ′ in the DTA samples were quantitatively analyzed, and the results are shown in Fig. 10. The average aspect ratio (length/width) of MC carbides for the cooling rates of 10 °C·min^{-1}, 30 °C·min^{-1}, and 90 °C·min^{-1} were calculated to be 2.36, 3.15, and 3.77, respectively. Based on the quantitative statistical results, the increasing cooling rate gradually reduces the average length and width of MC carbides, but has no obvious influence on the average area fraction, as shown in Fig. 10(a). The increasing cooling rate obviously decreases the average diameter of (γ+γ′) eutectics, but significantly increases its average area fraction [Fig. 10(b)]. Besides, the increasing cooling rate significantly reduces the average diameters of primary γ′ particles precipitated in both the interdendritic region and dendrite core [Fig. 10(c)].

In order to study the influential mechanism of cooling rate on the MC carbides, (γ+γ′) eutectics, and γ′ precipitation, the average compositions of dendrite core, interdendritic region, MC carbides, and (γ+γ′) eutectics in the DTA samples were analyzed using EDS, and the results are shown in Fig. 11. Note that experimental quantitative analysis of C is not feasible

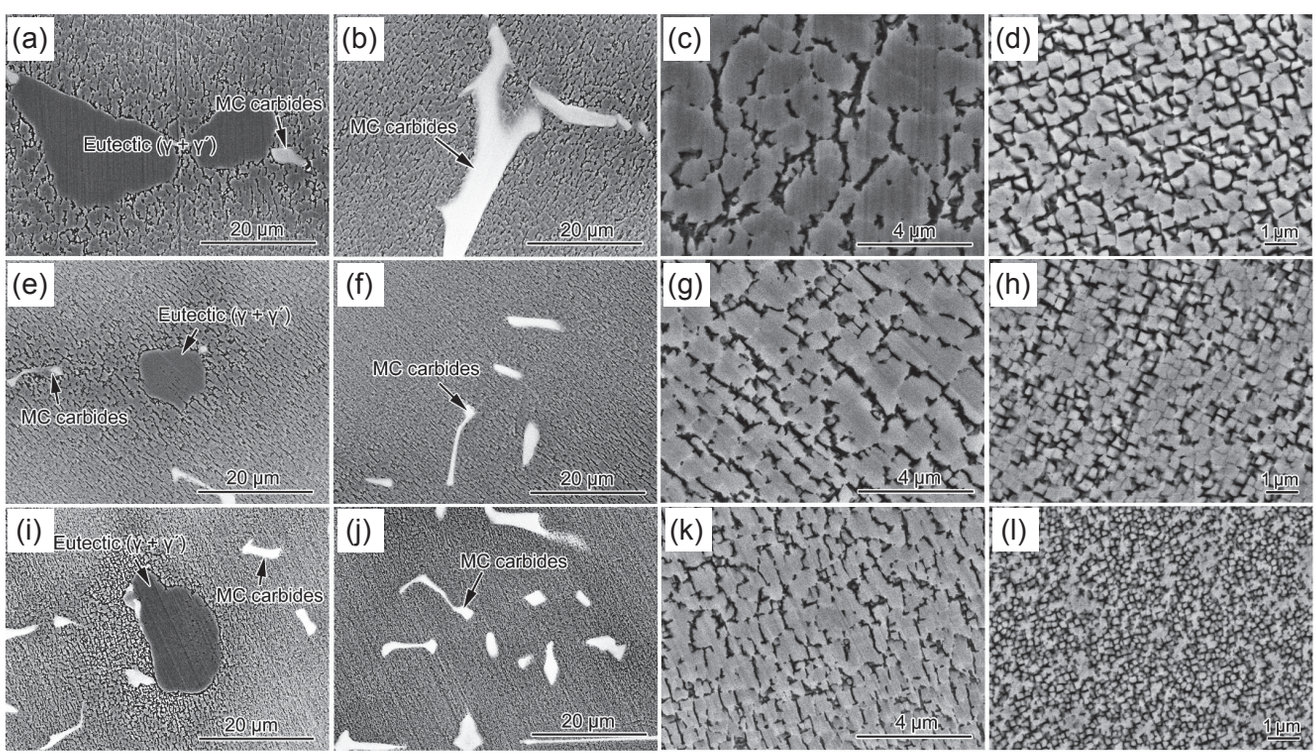

Fig. 9: SEM-BSE images showing the morphologies of precipitates in DTA samples with the cooling rates of 10 °C·min^{-1} (a, b, c, d), 30 °C·min^{-1} (e, f, g, h), and 90 °C·min^{-1} (i, j, k, l)

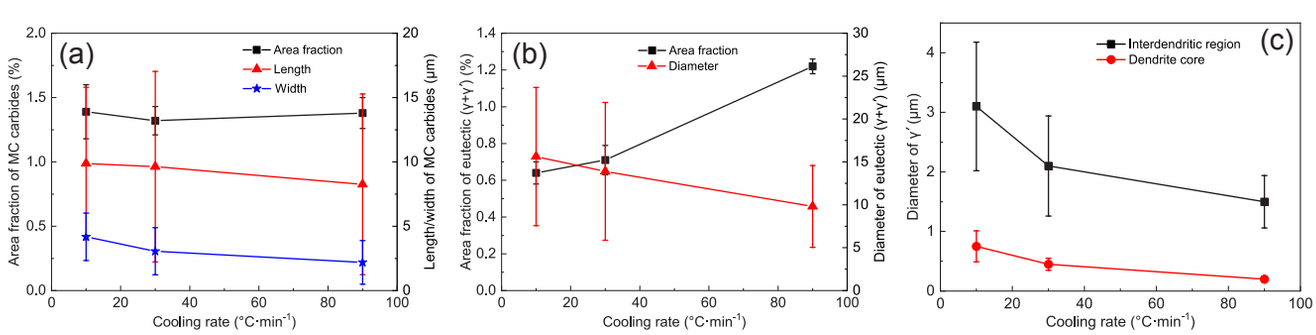

Fig. 10: Average area fractions and sizes of MC carbides (a), (γ+γ′) eutectics (b), and primary γ′ (c) in the DTA samples with different cooling rates

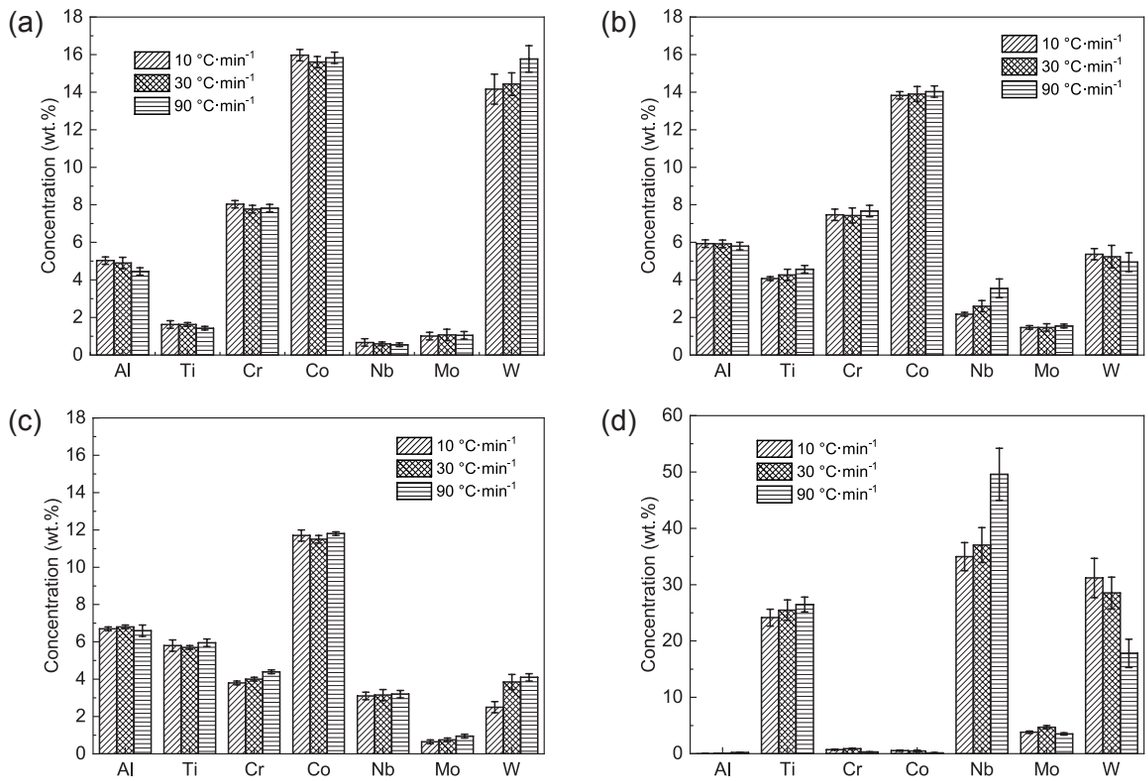

Fig. 11: Average concentrations of alloying elements in the dendrite core (a), interdendritic region (b), eutectic (γ+γ′) (c), and MC carbides (d)

because of surface contamination[33]. Under all the cooling conditions, the average concentrations of Al, Ti, and Nb increase gradually from the dendrite core to the interdendritic region and then to the (γ+γ′) eutectics, while those of Cr, Co, and W show an opposite trend. In addition, the average concentration of Mo firstly increases from the dendrite core to the interdendritic region, and then decreases from the interdendritic region to the (γ+γ′) eutectics. The increase of cooling rate obviously decreases the concentrations of Al, Ti, and Nb, markedly increases the concentration of W, but has no obvious influence on the concentrations of Cr, Co, and Mo in the dendrite core [Fig. 11(a)]. The increase of cooling rate obviously increases the concentrations of Ti and Nb, decreases the concentration of W, but has no obvious effect on those of Al, Cr, Co, and Mo in the interdendritic region [Fig. 11(b)]. The increase of cooling rate markedly increases the concentrations of Cr, Mo and W, but has no obvious influence on those of Al, Ti, Nb, and Co in the (γ+γ′) eutectics [Fig. 11(c)]. Moreover, the increase of cooling rate significantly increases the concentrations of Nb and Ti in the MC carbides, dramatically decreases the concentration of W, but has no obvious impact on the concentrations of the other alloying elements in MC carbides [Fig. 11(d)].

Figure 12 shows the effect of cooling rate on SRs of the alloying elements in solidified DTA samples. It can be seen that the Nb and Ti exhibit strong positive segregation, Al and Mo exhibit slight positive segregation, W exhibits strong negative segregation, but the Cr and Co tend to be distributed uniformly between the dendrite core and interdendritic region. The

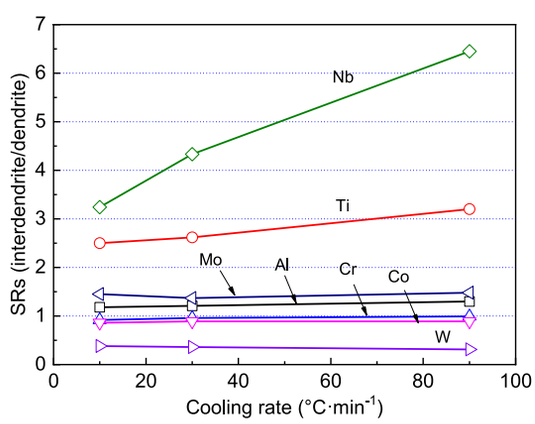

Fig. 12: Effect of cooling rates on segregation ratios (SRs) of the alloying elements in solidified DTA samples

increasing cooling rate obviously increases the SRs of Nb and Ti, slightly increases the SR of Al, slightly decreases the SR of W, but has little influence on the SRs of the other elements.

4 Discussion

With a decrease in the melt temperature, the MC carbides nucleate at first, acting as the nucleation sites for the γ dendrite. As the solidification proceeds, the γ dendrites grow continuously and the carbide forming elements Nb and Ti are gradually accumulated in the residual liquid. Consequently, this leads to the formation of additional MC carbides in the vicinity of the interdendritic region. Finally, the (γ+γ′) eutectics precipitate in the interdendritic region due to the segregation of Al and Ti in the liquid.

During the solidification, the back diffusion of alloying elements is an important factor that affects the micro-segregation[34]. Based on the Clyne-Kurz model which takes into account the solid-state back diffusion[35], the solute concentration in the liquid phase can be calculated using the following equations:

$$C_L = C_0\left[1-\left(1-2\Omega(\alpha)k\right)f_s\right]^{\frac{k-1}{1-2\Omega(\alpha)k}} \quad (3)$$

$$\Omega(\alpha) = \alpha\left[1-\exp\left(-\frac{1}{\alpha}\right)\right]-\frac{1}{2}\exp\left(-\frac{1}{2\alpha}\right) \quad (4)$$

$$\alpha = \frac{D_s t_f}{L^2} = \frac{4D_s\Delta T_f}{\lambda_2^2\dot{T}} \quad (5)$$

$$\Delta T_f = T_L - T_S \quad (6)$$

where C_L is the concentration of solute in liquid, C_0 is the initial solute concentration, $\Omega(\alpha)$ is a dimensionless parameter indicating the back-diffusion extent in solid, f_s is the solid fraction, k is the partition coefficient of alloying elements, D_s is the diffusion coefficient of alloying elements in solid, t_f is the local solidification time, L is the diffusion path length, $\dot{T}$ is the local cooling rate, ΔT_f is the solidification range, T_L is the liquidus temperature and and T_S is the solidus temperature.

The greater $\Omega(\alpha)$ value indicates larger back-diffusion extent[34]. Table 3 lists the calculated $\Omega(\alpha)$ values for the (γ+γ′) eutectic and MC carbide forming elements at various cooling rates. To improve the calculation accuracy, the D_s in Eq. (5) was calculated using the mid temperature (T_{mid}) between T_L and T_S. Relations of D_s values ($cm^2 \cdot s^{-1}$) for Al, Ti, Nb, W, C with the temperature are given as follows[36-41]:

$$D_{s,Al} = 0.75\exp\left(-284000/RT\right) \quad (7)$$

$$D_{s,Ti} = 0.00103\exp\left(-170300/RT\right) \quad (8)$$

$$D_{s,Nb} = 0.0053\exp\left(-236600/RT\right) \quad (9)$$

$$D_{s,W} = 0.43\exp\left(-312000/RT\right) \quad (10)$$

$$D_{s,C} = 0.0761\exp\left(-143511/RT\right) \quad (11)$$

where R is the gas constant (8.314 $J \cdot mol^{-1} \cdot K^{-1}$) and T is the temperature in Kelvin.

Table 3: Calculated $\Omega(\alpha)$ values of the (γ+γ′) eutectic and MC carbide forming elements at various cooling rates

Cooling rate	Al	Ti	Nb	W	C
10 °C·min^{-1}	1.12×10^{-2}	9.32×10^{-2}	2.99×10^{-3}	7.54×10^{-4}	54.16
30 °C·min^{-1}	1.05×10^{-2}	8.90×10^{-2}	2.76×10^{-3}	6.72×10^{-4}	51.55
90 °C·min^{-1}	9.23×10^{-3}	8.16×10^{-2}	2.54×10^{-3}	6.09×10^{-4}	47.96

It can be seen from Table 3 that the $\Omega(\alpha)$ values of these alloying elements decrease gradually with the increase of cooling rate, which suggests that the dilution influence of back diffusion on micro-segregation is weakened by the increasing cooling rate. Most likely, the influence of cooling rate on the back diffusion extent is considered to be the main reason why the SRs of positive segregation elements Al, Ti, and Nb become greater and that of negative segregation element W gets smaller as the cooling rate increases. The Al and Ti are the mainly forming elements for (γ+γ′) eutectics, and the increase in their segregation degrees naturally promotes the formation of (γ+γ′) eutectics, considering that the concentrations of these two elements in the (γ+γ′) eutectics are not obviously affected by the cooling rate. Thus, as the cooling rate increases, the area fraction of (γ+γ′) eutectics is enlarged significantly.

Since the diffusion coefficient of C in the solid is much greater than those of other alloying elements[42], it should be distributed uniformly in the γ dendrite during solidification[39, 43]. In this case, the impact level of back diffusion on the segregation degree of C will be extremely small and can be neglected, although the calculated $\Omega(\alpha)$ value of C decreases markedly with the increase of cooling rate. Moreover, the segregation degrees of MC carbides forming elements Nb and Ti are markedly increased by the increasing cooling rate, but the critical Nb and Ti concentrations for MC carbides formation are also increased. Thus, the area fraction of MC carbides is not markedly influenced by the increasing cooling rate.

According to the classic nucleation theory[31], the increasing cooling rate significantly increases the nucleation rates of precipitates. The MC carbides, (γ+γ′) eutectics, and primary γ′ have no enough time to fully grow under higher cooling rates, therefore, their average sizes decrease significantly with the increase of cooling rate[44]. In addition, the MC carbides and (γ+γ′) eutectics are mainly precipitated from interdendritic regions. The refinement of dendritic structures by the increasing cooling rate substantially increases the quantity of interdendritic regions but decreases their size, which not only provides more nucleation sites for the MC carbides and (γ+γ′) eutectics but also restricts their growth. This also contributes to variation of the sizes and quantities of these two non-equilibrium phases with increasing cooling rates.

5 Conclusions

This study aims to investigate the influence of cooing rate, ranging from 10 °C·min^{-1} to 90 °C·min^{-1}, on the solidification behavior and microstructure of high-alloyed GH4975 alloy. The main conclusions are as follows:

(1) The morphologies of MC carbides are mainly exhibit blocky and elongated shapes, while that of (γ+γ′) eutectics is ellipsoidal. The MC carbides can act as nucleation sites for the γ dendrites, and the γ dendrites nucleation becomes less dependent on the MC carbide primers as the cooling rate increases. As the solidification proceeds, more MC carbides precipitate near interdendritic regions and the solidification is terminated with (γ+γ′) eutectics precipitation.

(2) The increasing cooling rate obviously raises the liquidus temperature, reduces the solidus temperature, and hence enlarges the solidification range of GH4975 alloy. Besides, a higher cooling rate leads to a lower γ′ precipitation temperature.

(3) The solidification microstructure is obviously refined by the increase of cooling rate, and the SDAS, λ_2, as a function of cooling rate, $\dot{T}$, is experimentally evidenced as $\lambda_2 = 216.78\dot{T}^{-0.42}$.

(4) The average area fractions and sizes of MC carbides, (γ+γ′) eutectics, and primary γ′ have been quantitatively analyzed. As the cooling rate increases, the length and width of MC carbides markedly decrease, the aspect ratio of MC carbides increases, and the diameters of (γ+γ′) eutectics and primary γ′ significantly decrease. The increasing cooling rate obviously increases the area fraction of (γ+γ′) eutectics, but has no obvious influence on area fraction of MC carbides.

(5) The main reason for the influence of cooling rate on characteristics of MC carbides, (γ+γ′) eutectics, and primary γ′ is that the increasing cooling rate weakens the back diffusion of Al, Ti and Nb, increases the undercooling, limits the growth of these phases, and refines the dendritic structure.

Acknowledgments

This work was financially supported by the National Natural Science Foundation of China (Grant Nos. 52474362, 52174317 and 51904146) and the General Project Funded by Liaoning Province Education Department (Grant No. JYTMS20230943).

Conflict of interest

The authors declare that they have no conflict of interest.

References

[1] Jiang H, Dong J X, Zhang M C, et al. Development of typical hard-to-deform nickel-base superalloy for turbine disk served above 800 °C. Aeronautical Manufacturing Technology, 2021, 64(1/2): 62–73.

[2] Zhang B J, Zhao G P, Zhang W Y, et al. Investigation of high performance disc alloy GH4065 and associated advanced processing techniques. Acta Metallurgica Sinica, 2015, 51(10): 1227–1234.

[3] Zhang Y, Li X X, Wei K, et al. Hot deformation characteristics of novel wrought superalloy GH4975 extruded rod used for 850 °C turbine disc. Acta Metallurgica Sinica, 2020, 56(10): 1401–1410.

[4] Li Y, Dong Y, Jiang Z, et al. Study on microsegregation and homogenization process of a novel nickel-based wrought superalloy. Journal of Materials Research and Technology, 2022, 19: 3366–3379.

[5] Xiang X M, Jiang H, Dong J X, et al. As-cast microstructure characteristic and homogenization of a newly developed hard-deformed Ni-based superalloy GH4975. Acta Metallurgica Sinica, 2020, 56(7): 988–996.

[6] Zhao G D, Liu F, Zang X M, et al. Microstructure and hot ductility behavior of Ni-based superalloy U720Li with boron addition. Rare Metals, 2021, 40: 1145–1154.

[7] Whitesell H S, Overfelt R A. Influence of solidification variables on the microstructure, macrosegregation, and porosity of directionally solidified Mar-M247. Materials Science and Engineering: A, 2001, 318(1–2): 264–276.

[8] Zhao G D, Yu L X, Yang G L, et al. The role of boron in modifying the solidification and microstructure of nickel-base alloy U720Li. Journal of Alloys and Compounds, 2016, 686: 194–203.

[9] Yu J, Sun X, Zhao N, et al. Effect of heat treatment on microstructure and stress rupture life of DD32 single crystal Ni-base superalloy. Materials Science and Engineering: A, 2007, 460: 420–427.

[10] Chen Q, Jones N, Knowles D. The microstructures of base/modified RR2072 SX superalloys and their effects on creep properties at elevated temperatures. Acta Materialia, 2002, 50(5): 1095–1112.

[11] Zhao G D, Zang X M, Sun W R. Role of carbon in modifying solidification and microstructure of a Ni-based superalloy with high Al and Ti contents. Journal of Iron and Steel Research International, 2021, 28: 98–110.

[12] Gong L, Chen B, Zhang L, et al. Effect of cooling rate on microstructure, microsegregation and mechanical properties of cast Ni-based superalloy K417G. Journal of Materials Science and Technology, 2018, 34(5): 811–820.

[13] El-Bagoury N, Yamamoto K, Miyahara H, et al. Influence of rhenium and cooling rate on the solidification of Ni base superalloys, Inconel 718. Materials Transactions, 2005, 46(5): 909–915.

[14] Milenkovic S, Sabirov I, LLorca J. Effect of the cooling rate on microstructure and hardness of MAR-M247 Ni-based superalloy. Materials Letters, 2012, 73: 216–219.

[15] Ling L, Han Y, Zhou W, et al. Study of microsegregation and Laves phase in Inconel718 superalloy regarding cooling rate during solidification. Metallurgical and Materials Transactions: A, 2015, 46(1): 354–361.

[16] Shi X, Duan S C, Yang W S, et al. Effect of cooling rate on microsegregation during solidification of superalloy Inconel 718 under slow-cooled conditions. Metallurgical and Materials Transactions: B, 2018, 49: 1883–1897.

[17] Long Z, Liu X, Yang W, et al. Thermodynamic assessment of liquid composition change during solidification and its effect on freckle formation in superalloys. Materials Science and Engineering: A, 2004, 386(1–2): 254–261.

[18] Voort G. Metallography: Principles and practice. McGraw-Hill, New York, 1984. https://doi.org/10.1016/0026-0800(85)90051-5.

[19] Hobbs R, Tin S, Rae C. A castability model based on elemental solid-liquid partitioning in advanced nickel-base single-crystal superalloys. Metallurgical and Materials Transactions: A, 2005, 36(10): 2761–2773.

[20] Monajati H, Taheri A, Jahazi M, et al. Deformation characteristics of isothermally forged UDIMET 720 nickel-base superalloy. Metallurgical and Materials Transactions: A, 2005, 36(4): 895–905.

[21] Zhao G D, Zang M X, Sun W R. Role of carbon in modifying solidification and microstructure of a Ni-based superalloy with high Al and Ti contents. Journal of Iron and Steel Research International, 2021, 28: 98–110.

[22] Ghaemifar S, Mirzadeh H. Precipitation kinetics of niobium carbide (NbC) during homogenization heat treatment of additively manufactured Inconel 718 superalloy. Journal of Materials Research and Technology, 2023, 25: 1774–1781.

[23] Ferreri N C, Vogel S C, Knezevic M. Determining volume fractions of γ, γ′, γ″, δ, and MC-carbide phases in Inconel 718 as a function of its processing history using an advanced neutron diffraction procedure. Materials Science and Engineering: A, 2020, 781: 139228.
[24] Hosseini V, Shabestari S, Gholizadeh R. Study on the effect of cooling rate on the solidification parameters, microstructure, and mechanical properties of LM13 alloy using cooling curve thermal analysis technique. Materials & Design, 2013, 50: 7–14.
[25] Dobrzański L, Maniara R, Sokołowski J, et al. Effect of cooling rate on the solidification behavior of AC AlSi7Cu2 alloy. Journal of Materials Processing Technology, 2007, 191(1–3): 317–320.
[26] Dobrzański L, Maniara R, Sokolowski J. The effect of cast Al-Si-Cu alloy solidification rate on alloy thermal characteristics. Journal of Achievements in Materials and Manufacturing Engineering, 2006, 17(1–2): 217–220.
[27] Zhang Y, Li Z, Nie P, et al. Effect of cooling rate on the microstructure of laser-remelted INCONEL 718 coating. Metallurgical and Materials Transactions: A, 2013, 44: 5513–5521.
[28] Yi P, Liu Y, Shi Y, et al. Effects analysis of ambient conditions on process of laser surface melting. Optics & Laser Technology, 2011, 43(8): 1411–1419.
[29] Zhao G D, Zang X M, Li W M, et al. Study on primary carbides precipitation in H13 tool steel regarding cooling rate during solidification. China Foundry, 2020, 17(3): 235–244.
[30] Matache G, Stefanescu D, Puscasu C, et al. Dendritic segregation and arm spacing in directionally solidified CMSX-4 superalloy. International Journal of Cast Metals Research, 2016, 29(5): 303–316.
[31] Kurz W, Fisher D J, Rappaz M. Fundamentals of solidification, 5th edition. Trans. Tech. Publications Limited, 2023. https://doi.org/10.4028/b-v7b35q.
[32] Quaresma J M, Santos C A, Garcia A, et al. Correlation between unsteady-state solidification conditions, dendrite spacings, and mechanical properties of Al-Cu alloys. Metallurgical and Materials Transactions: A, 2000, 31: 3167–3178.
[33] Lippard H, Campbell C, Dravid V, et al. Microsegregation behavior during solidification and homogenization of AerMet100 steel. Metallurgical and Materials Transactions: B, 1998, 29: 205–210.
[34] Seo S, Lee J, Yoo Y, et al. A comparative study of the γ/γ′ eutectic evolution during the solidification of Ni-base superalloys. Metallurgical and Materials Transactions: A, 2011, 42(10): 3150–3159.
[35] Clyne T, Kurz W. Solute redistribution during solidification with rapid solid state diffusion. Metallurgical Transactions: A, 1981, 12(6): 965–971.
[36] Epishin A, Chyrkin A, Nolze G, et al. Interdiffusion in the face-centered cubic phase of the Co-Al-W-Ta system between 1090 and 1240 °C. Journal of Phase Equilibria and Diffusion, 2018, 39: 176–185.
[37] Sohrabi M J, Mirzadeh H. Revisiting the diffusion of niobium in an as-cast nickel-based superalloy during annealing at elevated temperatures. Metals and Materials International, 2020, 26: 326–332.
[38] Aleman B, Gutierrez I, Urcola J. Interface microstructures in the diffusion bonding of a titanium alloy Ti 6242 to an Inconel 625. Metallurgical and Materials Transactions: A, 1995, 26: 437–446.
[39] Meng Y, Thomas B G. Heat-transfer and solidification model of continuous slab casting: CON1D. Metallurgical and Materials Transactions: B, 2003, 34: 685–705.
[40] Ueshima Y, Mizoguchi S, Matsumiya T, et al. Analysis of solute distribution in dendrites of carbon steel with δ/γ transformation during solidification. Metallurgical Transactions: B, 1986, 17: 845–859.
[41] Mao M, Guo H, Wang F, et al. Effect of cooling rate on the solidification microstructure and characteristics of primary carbides in H13 steel. ISIJ International, 2019, 59(5): 848–857.
[42] Flemings M C. Solidification processing. Metallurgical and Materials Transactions: B, 1974, 5: 2121–2134.
[43] Shulga A. Boron and carbon behavior in the cast Ni-base superalloy EP962. Journal of Alloys and Compounds, 2007, 436(1–2): 155–160.
[44] Luo Y, Guo H, Guo J. Effect of cooling rate on the transformation characteristics and precipitation behaviour of carbides in AISI M42 high-speed steel. Ironmaking & Steelmaking, 2019, 46(7): 698–704.